Behavior and Sensitivity of Phase Arrival Times (PHASE)

Emmanuel Skarsoulis
Foundation for Research and Technology Hellas
Institute of Applied and Computational Mathematics
100 N. Plastira str., GR-70013 Heraklion, Greece
phone: +30-2810-391776 fax: +30-2810-391801
email: eskars@iacm.forth.gr

in collaboration with

Bruce Cornuelle and Matthew Dzieciuch
Scripps Institution of Oceanography
University of California, San Diego
La Jolla, CA 92093-0225
phone: (858) 534-4021 fax: (858) 534-9820
email: bdc@ucsd.edu, mad@uscd.edu

Award Number: N00014-13-1-0366
http://www.iacm.forth.gr, http://sio.ucsd.edu

LONG-TERM GOALS

Our long-term goal is to study the sensitivity behavior of acoustic phase arrival times, as an alternative observable offering increased resolution (compared to peak arrivals), for the recovery of sound-speed perturbations in the ocean.

OBJECTIVES

The objective of this work is to study the behavior and sensitivity of ocean acoustic phase arrival times due to sound-speed changes, in comparison to those of peak arrival times. The aim is to derive perturbation relations and sensitivity kernels connecting sound-speed and travel-time perturbations, and, further, to study the behavior of phase arrival times and its predictability, depending on propagation and signal characteristics.

APPROACH

Phase arrival times are mathematically modeled as stationary points - times of constant phase - of the acoustic pressure. Using this definition, expressions for the corresponding travel-time perturbations are derived and the sensitivity behavior of phase arrival times, due to sound speed changes, is studied. The resulting sensitivity kernels (Born-Frechet kernels) for phase arrival times are compared to the corresponding travel-time sensitivity kernels for peak arrivals.

WORK COMPLETED

Up to the present the following tasks have been completed: Mathematical modeling of finite-frequency phase arrival times and derivation of perturbation expressions. Derivation of 1D, 2D and 3D sensitivity

kernels for phase arrival times and comparison with travel-time sensitivity kernels for peak arrivals. Comparison of actual vs. predicted (based on perturbation expressions and sensitivity kernels) displacements of phase and peak arrivals.

RESULTS

Mathematical modeling and perturbation expressions

The complex pressure at the receiver in the time domain [1] can be written in the form

$$p(t) = a(t)e^{i\varphi(t)}e^{i\omega_0 t}, \tag{1}$$

where t denotes time, $a(t)$ is the amplitude (arrival pattern), $\varphi(t)$ is the phase and ω_0 is the central (carrier) circular frequency of the source. The demodulated pressure results after removal of the carrier frequency and can alternatively be expressed in terms of its real and imaginary parts, $u(t)$ and $v(t)$:

$$\tilde{p}(t) = a(t)e^{i\varphi(t)} = u(t) + iv(t) \tag{2}$$

The above quantities $a(t)$, $\varphi(t)$, u(t), and $v(t)$ depend on the source/receiver location as well as on the sound-speed distribution $c(\mathbf{x})$, where $\mathbf{x}$ is the spatial variable. Thus, perturbations $\delta c(\mathbf{x})$ of the sound speed give rise to perturbations in arrival amplitude, arrival phase and arrival times. Peak arrival times are defined as the times of the local maxima (peak arrivals) of the arrival pattern: $\dot{a}(\tau_P; c) = 0$. As the sound speed changes the peaks of the arrival pattern are deformed and displaced, i.e. peak arrival times change as well. The resulting perturbation relations reads [1]

$$\delta\tau_P = -\frac{\delta\dot{a}_1(\tau_P; c; \delta c)}{\ddot{a}(\tau_P; c)} = -\frac{\dot{u}\delta u_1 + u\delta\dot{u}_1 + \dot{v}\delta v_1 + v\delta\dot{v}_1}{\dot{u}^2 + u\ddot{u} + \dot{v}^2 + v\ddot{v}}, \tag{3}$$

where the quantities u , v and their time derivatives are considered at the background state (c) and their 1st-order perturbations are due to δc.

Phase arrival times can be defined in different ways for the complex pressure $p(t)$ or for its demodulated form $\tilde{p}(t)$. In the following phase arrival times on the modulated pressure are considered – for demodulated phase arrival times see Ref. [3]. The modulated phase can be written as

$$\psi(t) = \varphi(t) + \omega_0 t \tag{4}$$

Due to the term $\omega_0 t$, the phase $\psi(t)$ is rapidly increasing with time. Phase arrival times τ_ψ are defined as fixed-level crossings of the modulated phase $\psi(\tau_\psi) = \gamma$, where γ is a fixed threshold (e.g. $\gamma = 2n\pi$ corresponds to maxima, $\gamma = \pi/2 + 2n\pi$ to zero crossings of the real part of $p(t)$). By applying the definition at the background and perturbed state and using a Taylor expansion of the latter we obtain

$$\delta\tau_\psi = -\frac{\delta\varphi}{\dot{\varphi} + \omega_0} = -\frac{u\delta v - v\delta u}{u\dot{v} - v\dot{u} + \omega_0\left(u^2 + v^2\right)} \tag{5}$$

By comparing eqs. (3) and (5) we see that the perturbation expressions for peak and phase arrival are different, so the two time observables will behave differently, in general. This is quite anticipated since

the two observables correspond to different functions, peak arrival times to the amplitude function $a(t)$ and phase arrival times to the phase function $\psi(t)$.

Sensitivity kernels of phase arrival times

The complex pressure p at the receiver in the time domain, and its perturbation δp due to perturbations of the sound speed distribution, can be expressed through the inverse Fourier transform in terms of the signal $P_s(\omega)$ emitted by the source in the frequency domain and the frequency-domain Green's function $G_{sr}(\omega;c;\mathbf{x}_r|\mathbf{x}_s)$ and its perturbation $\delta G_{sr}(\omega;c;\delta c;\mathbf{x}_r|\mathbf{x}_s)$, respectively

$$p(t)=\frac{1}{2\pi}\int_{-\infty}^{+\infty}P_s(\omega)G(\omega;c;\mathbf{x}_r|\mathbf{x}_s)e^{i\omega t}d\omega \quad \text{and} \quad \delta p(t)=\frac{1}{2\pi}\int_{-\infty}^{+\infty}P_s(\omega)\delta G(\omega;c;\delta c;\mathbf{x}_r|\mathbf{x}_s)e^{i\omega t}d\omega \tag{6}$$

where $\mathbf{x}_s$ and $\mathbf{x}_r$ is the source and receiver position vector. The perturbation of the Green's function can be expressed through the first Born approximation [1], which in 3-dimensional space reads

$$\delta G_{3D}(\omega;c;\delta c;\mathbf{x}_r|\mathbf{x}_s)=-2\omega^2\iiint_V G_{3D}(\omega;c;\mathbf{x}|\mathbf{x}_s)G_{3D}(\omega;c;\mathbf{x}_r|\mathbf{x})\frac{\delta c(\mathbf{x})}{c^3(\mathbf{x})}dV(\mathbf{x}). \tag{7}$$

Assuming a range-independent background environment the 3-dimensional Green's function can be written in terms of normal modes [2]

$$G_{3D}(r,z\,|\,z_s)=\frac{e^{-i\pi/4}}{\rho_W\sqrt{8\pi}}\sum_{m=1}^{M}\frac{\varphi_m(z_s)\varphi_m(z)}{\sqrt{k_m r}}e^{-ik_m r}, \tag{8}$$

where ρ_W is the water density and k_m and $\varphi_m(z)$ are the real eigenvalues and the corresponding eigenfunctions of the vertical Sturm-Liouville problem. By substituting eq. (8) into eq. (7) and using the perturbation relations, eqs. (3) and (5), expressions of the form

$$\delta\tau=\iiint_V K_\tau^{(3D)}(\mathbf{x})\delta c(\mathbf{x})dV(\mathbf{x}) \tag{9}$$

can be obtained, where $K_\tau^{(3D)}(\mathbf{x})$ is the corresponding 3-dimensional travel-time sensitivity kernel, describing the effect that a sound-speed perturbation at location $\mathbf{x}$ will have on the travel time τ of interest. A similar expression can be obtained for the 2-dimensional sensitivity kernel based on the 2-dimensional Green's function [2].

The 1-dimensional vertical sensitivity kernel, corresponding to range-independent sound-speed perturbations, can be obtained by applying perturbation theory to the vertical Sturm-Liouville problem. The resulting perturbation expression for the 3-dimensional Green's function, eq. (8), reads

$$\delta G_{3D}=\frac{e^{-i\pi/4}}{\rho_W\sqrt{8\pi}}\sum_{m=1}^{M}\left[\sum_{\substack{n=1\\n\neq m}}^{M}\frac{Q_{mn}U_{mn}}{\Lambda_{mn}}+\left(\frac{1}{2k_m}+ir\right)\frac{U_{mm}Q_{mm}}{k_m}\right]\frac{e^{-ik_m r}}{\sqrt{k_m r}}, \tag{10}$$

where $\Lambda_{mn}=k_m^2-k_n^2$ and

$$Q_{mn} = -2\omega^2 \int_0^h \frac{\varphi_m(z')\varphi_n(z')}{c^3(z')} \Delta c(z') dz' \quad , \quad U_{mn} = \begin{cases} \varphi_m(z_S)\varphi_n(z) + \varphi_n(z_S)\varphi_m(z) \ , & n \neq m \\ -\frac{1}{2}\varphi_m(z_S)\varphi_m(z) \ , & n = m \end{cases} \tag{11}$$

where h is the water depth. By combining this with the perturbation relations, eqs. (3) and (5), expressions can be obtained for the travel-time perturbations of the form

$$\delta\tau = \int_0^h K_\tau^{(1D)}(z)\delta c(z) dz \tag{12}$$

where $K_\tau^{(1D)}(z)$ is the corresponding 1-dimensional (vertical) sensitivity kernel, describing the effect that a change of the sound-speed profile at depth z will have on the travel time τ of interest.

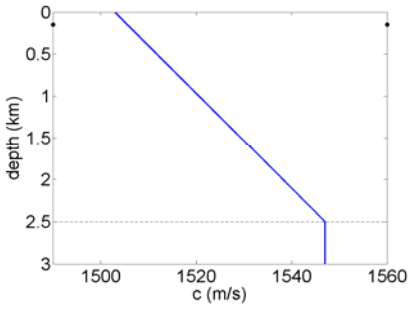

Fig. 1. Linear sound-speed profile

Some numerical results for travel-time sensitivity kernels of peak and phase arrival times are presented in the following. A simple deep-water environment characterized by a linear sound-speed profile, see Fig. 1, is selected. Source and receiver are taken at a depth of 150 m and horizontal distance of 30 km, whereas the water is 2500 m deep, bounded by an absorbing bottom. The acoustic signal is a Gaussian pulse with central frequency 100 Hz and bandwidth 70 Hz (3-dB bandwidth).

Fig. 2 shows at the top the 3D arrival pattern on the left and the pressure at the receiver in the time domain (real part) on the right. The lower panels show sections of the 3D travel-time sensitivity kernels corresponding to the 3 marked peaks (peak arrival times on the left and phase arrival times on the right) – sections with the vertical plane through the source and the receiver. The 3D arrival pattern contains six major peaks, the first three of which can be resolved as ray arrivals. The real part of the pressure on the right shows a modulated version of the arrival pattern with modulation frequency corresponding to the central source frequency, 100 Hz. The 3 marked phase arrivals on the right are selected to be closest – in time – to the selected 3 peak arrivals on the left.

The sensitivity kernels of the peak arrival times are concentrated about the acoustic paths connecting the source and the receiver. Arrival 1 corresponds to a steep path with lower turning depth about 1300 m – there is no upper turning depth since the sound speed profile is upward refracting. Later arrivals 2 and 3 correspond to gradually shallower paths. The last arrival samples the upper 200m, with turning depth very close to the source/receiver depth (150 m). The situation is very similar in the case of the sensitivity kernels of the phase arrival times on the right. The travel-time sensitivity is prevailingly negative (blue color), still there are areas of positive sensitivity as well. The vertical extent of the sensitivity kernel appears slightly larger in the case of phase arrival times. Further the phase arrival time sensitivity values are larger.

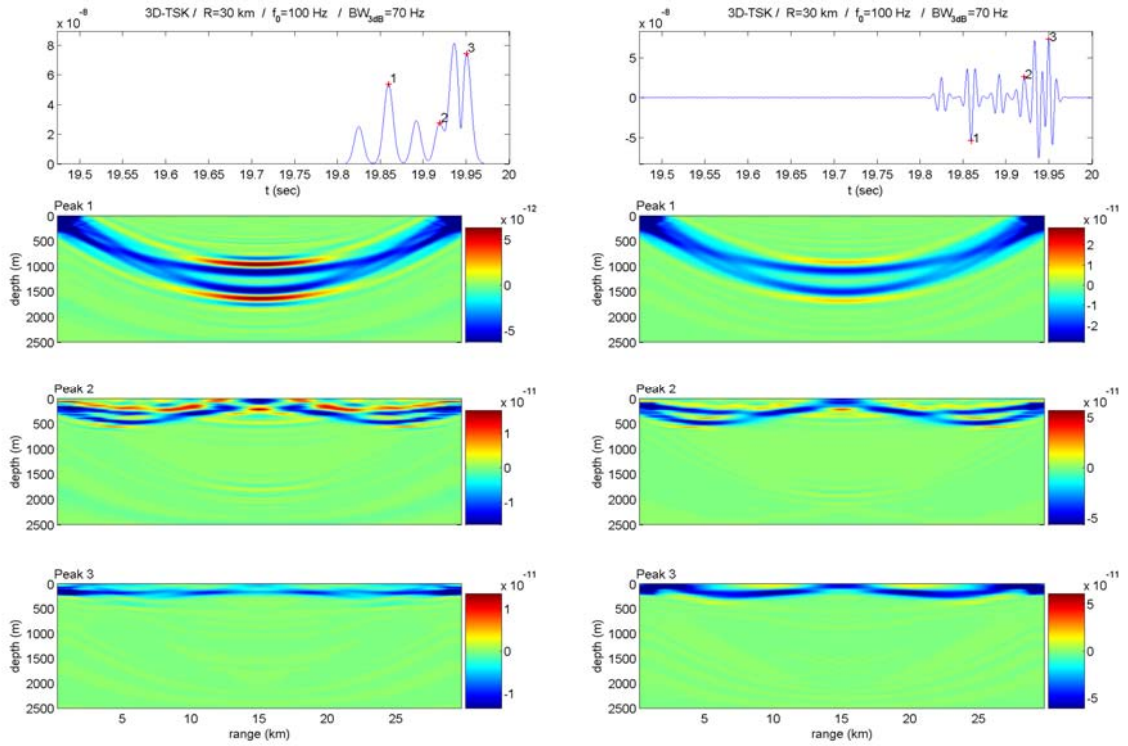

Fig. 2. 3D propagation results at 30 km range. Left: Arrival pattern (top) and sensitivity kernels (lower) for peak arrival times of marked peaks. Right: Acoustic pressure (top) and sensitivity kernels (lower) for phase arrival times of marked peaks.

Fig. 3. Shows the corresponding propagation and sensitivity results based on the 2D Green's function [2]. The arrival patterns are very similar to the 3D results of Fig. 1 even though there are small differences, mainly in the amplitudes. The 2D sensitivity kernels are limited on the 2D plane, and as it has been shown [2] they equal the marginals of the 3D kernels (integrals in the horizontal cross-range direction). The vertical sensitivity extent of the phase arrival times, on the right, appears to be significantly broader than that of the peak arrival times on the left. On the other hand, the sensitivity magnitudes of the two observables are comparable. Apparently, the large negative sensitivity values of the phase arrival times on the source/receiver vertical plane in Fig. 2 are compensated by the off-plane behavior. Fig. 4 shows the vertical sensitivity kernels (1D) of the peak arrival times, on the left, and phase arrival times, on the right, of the 3 peaks marked in Fig. 1. The calculations are based on the 3D Green's function in a range-independent environment. The vertical extent of the travel-time sensitivity is larger in the case of phase arrival times (the high-sensitivity interval is broader), compared to that of peak arrival times. This is seen more clearly in the case of the last peak (bottom panels in Fig. 4). On the other hand the sensitivity magnitudes are comparable, and they are much larger for the late than for the early arrivals – note the different scales in the horizontal and vertical axes of the top panels in Fig. 4. From these figures it becomes clear that the sensitivity behavior of the phase and peak arrival times is different. Even though the differences are small, they can cause large deviations in travel time behavior depending on the support of the sound-speed perturbations.

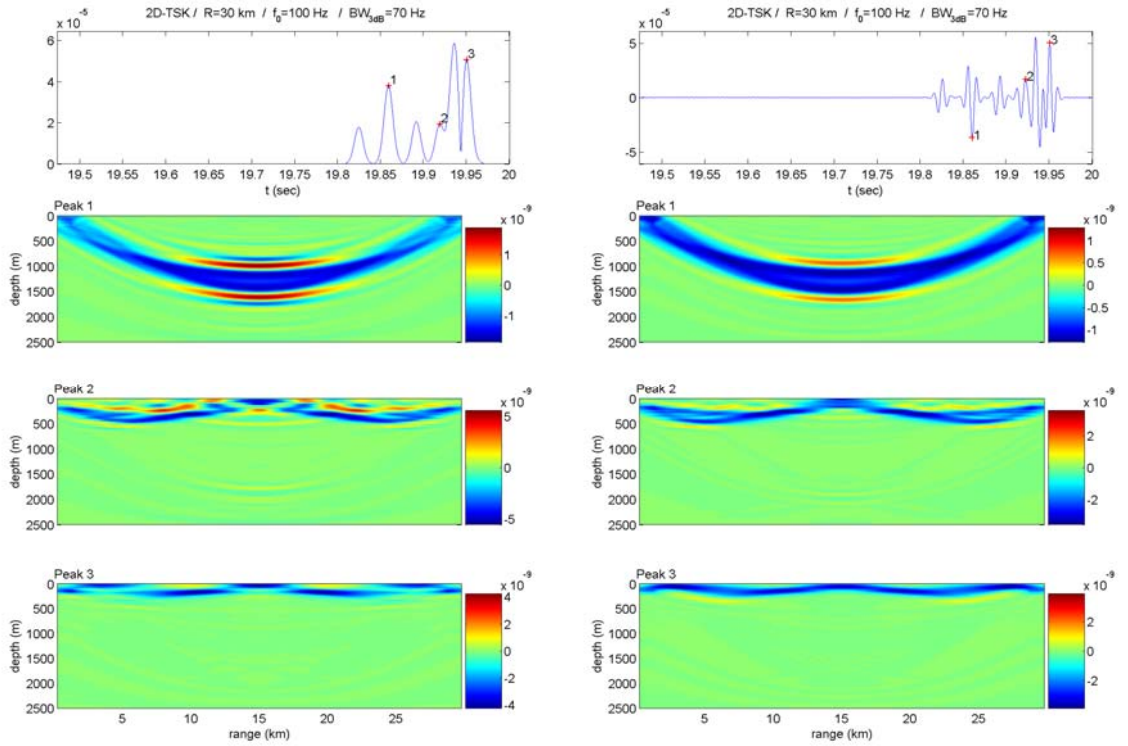

Fig. 3. 2D propagation results at 30 km range. Left: Arrival pattern (top) and sensitivity kernels (lower) for peak arrival times of marked peaks. Right: Acoustic pressure (top) and sensitivity kernels (lower) for phase arrival times of marked peaks.

<u>Comparison of actual vs. predicted displacements of phase arrivals</u>

In the following, some results from the perturbation study of peak and phase arrivals are presented. The focus is on the predictability of actual perturbations using the vertical travel-time sensitivity and applying it directly on the sound-speed perturbations. Box-shaped sound-speed perturbations with vertical extent 100 m. Fig. 5 shows the actual travel-time perturbations of peak 1 (crosses) caused by sound-speed changes about the depth of 1400 m, close to the maximum sensitivity depth, in comparison with the 1st-order predictions based on the corresponding sensitivity kernels (solid lines). The predictions turn out to be successful in both cases, with the phase arrival times exhibiting slightly weaker perturbations, in agreement with the weaker sensitivity kernel in Fig. 4.

Fig. 6 shows travel-time perturbations of peak 3 caused by sound-speed changes centred about the depth of 150 m, close to the maximum sensitivity depth. Even though the sound-speed perturbations are of the same vertical extent and magnitude as before the travel-time perturbations are much larger (note the different scales in the vertical axes in Figs. 5 and 6). The predictions based on the sensitivity kernels (solid lines) are again in good agreement with the actual travel-time perturbations (crosses) for both observables. The perturbation behavior of phase and peak arrival times is almost identical in this case and this is in agreement with the very similar magnitude of the corresponding sensitivity kernels in Fig. 4 (bottom panels) at the depth of 150 m.

In order to check the sufficiency of the sensitivity kernel description we select to apply perturbations around the depth of 100 m where the two kernels are different – the one for the phase arrival time takes

a value close to its negative maximum, whereas the kernel of the peak arrival times is much smaller. The results are shown in Fig. 7 and we see that the phase arrival time perturbations are nearly of the same magnitude as before, whereas those of peak arrival times are much weaker. The perturbation prediction based on the sensitivity kernels (solid lines) is good.

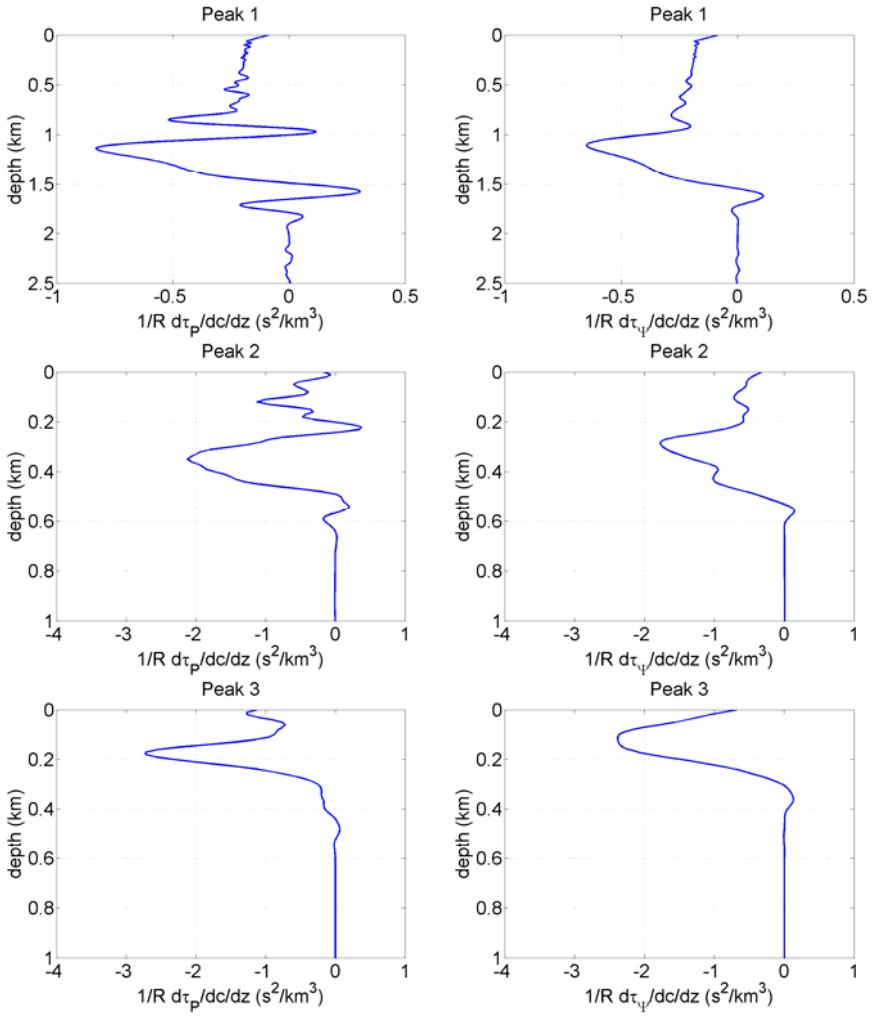

Fig. 4: Normalized vertical sensitivity kernels for peak arrival times (left) and phase arrival times (right) of the 3 peaks marked in Fig. 2.

IMPACT/APPLICATIONS

The phase arrival times offer higher temporal resolution than peak arrivals, since their width is controlled by the central source frequency rather than the source bandwidth. Furthermore, while peak arrivals require broadband (low-Q) sources, phase arrivals can be resolved even in the case of smaller bandwidths, which means cheaper sources. The sensitivity and perturbation behavior of phase arrivals is in general different from that of peak arrivals, and large deviations may occur between the perturbations of the two observables, depending on the location (the spatial support) of the underlying sound-speed change. Phase arrival times exhibit good predictability in the studied cases, i.e. the first-order predictions based on the sensitivity kernels lie close to the actual time perturbations. Thus, phase

arrival times offer a useful alternative to peak arrivals as observables for ocean acoustic tomography. The exploitation of peak arrival times requires dense sampling in time, in order to keep track of the phase (2π-ambiguity) as the ocean (sound speed) changes.

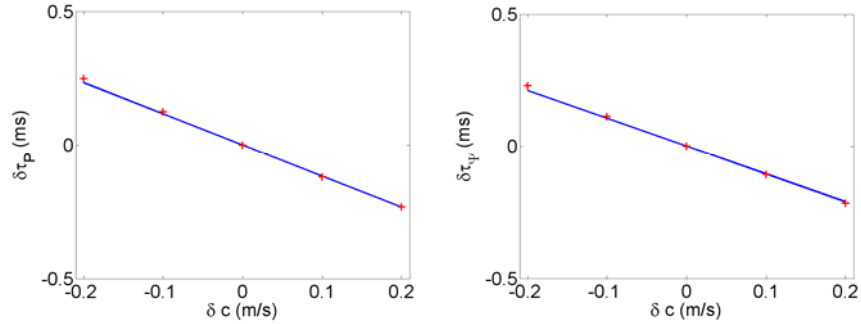

Fig. 5: Actual (+) and predicted (line) travel-time perturbations for peak (left) and phase (right) arrival times for arrival 1 and sound-speed perturbations about 1400 m depth

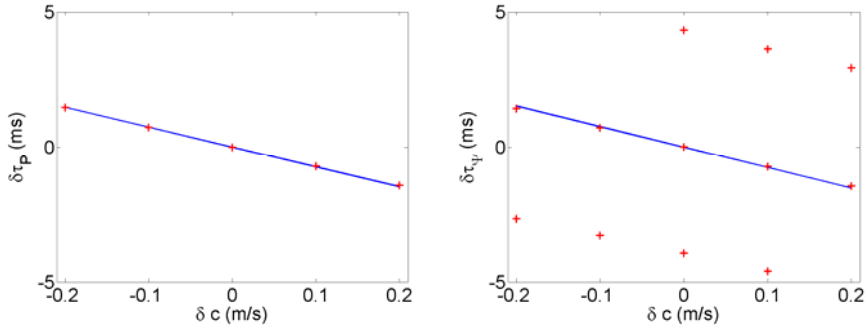

Fig. 6: Actual (+) and predicted (line) travel-time perturbations for peak (left) and phase (right) arrival times for arrival 3 and sound-speed perturbations about 150 m depth

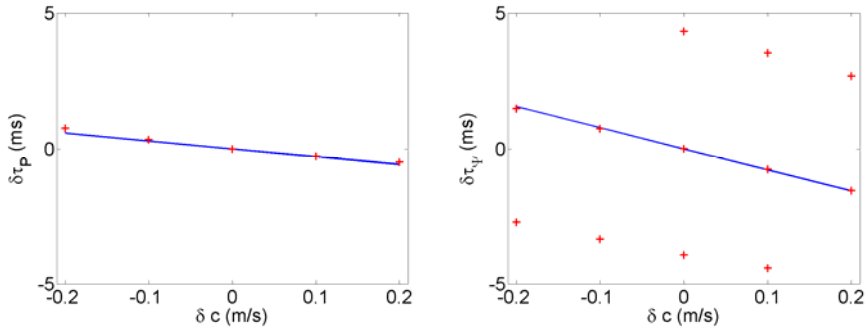

Fig. 7: Actual (+) and predicted (line) travel-time perturbations for peak (left) and phase (right) arrival times for arrival 3 and sound-speed perturbations about 100 m depth

RELATED PROJECTS

In the framework of NPAL (ONR contract N000140310182) Bruce Cornuelle and Matthew Dzieciuch have been exploring travel-time sensitivity kernels in range-dependent ocean environments.

REFERENCES

[1] E.K. Skarsoulis, B.D. Cornuelle, 'Travel-time sensitivity kernels in ocean acoustic tomography', *J. Acoust. Soc. Am*. 116, pp. 227-238, 2004.

[2] E.K. Skarsoulis, B.D. Cornuelle, M.A. Dzieciuch, Travel-time sensitivity kernels in long-range propagation, *Journal of the Acoustical Society of America*, Vol. 126, pp. 2223-2233, 2009

PUBLICATIONS

[3] E.K. Skarsoulis, B.D. Cornuelle, M.A. Dzieciuch, Sensitivity behavior of phase and peak arrival times, in Proc. 1st Underwater Acoustics Conference, Corfu, 24-28 June 2013

[4] E.K. Skarsoulis, B.D. Cornuelle, M.A. Dzieciuch, Long-range asymptotic behavior of vertical travel-time sensitivity kernels, *Journal of the Acoustical Society of America*, in print, 2013.

[5] M.A. Dzieciuch, B.D. Cornuelle, E.K. Skarsoulis, Structure and stability of wave-theoretic kernels in the ocean, *Journal of the Acoustical Society of America*, in print, 2013.